

Dynamics of the Measurement of Nuclear Spins in a Solid-State Quantum Computer

Gennady P. Berman^a, David K. Campbell^{a,b}, Gary D. Doolen^a, and Kirill E. Nagaev^d

^aTheoretical Division and CNLS, Los Alamos National Laboratory, Los Alamos, NM 87545

^bDepartment of Physics, University of Illinois at Urbana-Champaign, 1110 West Green St., Urbana, IL 61801-3080

^dInstitute of Radio Engineering and Electronics, Russian Academy of Sciences, Mokhovaya St. 11, 103907 Moscow, Russia

We study numerically the process of nuclear spin measurement in a solid-state quantum computer of the type proposed by Kane by modeling the quantum dynamics of two coupled nuclear spins on ³¹P donors implanted in silicon. We estimate the minimum measurement time necessary for the reliable transfer of quantum information from the nuclear spin subsystem to the electronic subsystem. We also calculate the probability of error for typical values of the external noise.

I. INTRODUCTION

Recently, a new implementation of a solid-state quantum computer was proposed by Kane¹. Kane's idea is to realize the quantum qubits by using the nuclear spins of ³¹P donors in silicon. These $S=1/2$ spins are known to exhibit very long relaxation times because of their weak coupling to the environment². At low temperatures, when there are no thermally excited electrons in the conduction band, this contact is mediated primarily by the magnetic field and the hyperfine interaction with s -electrons localized on the donor. However not all s -electrons are equally important for this mediation. The electrons in the inner shells are localized within one lattice cell and are also very weakly coupled to the environment. Of the five outer ($3p$) electrons in a P atom (one more than Si), four form valence bonds with surrounding Si atoms, while the fifth is given off to the conduction band to form a loosely bound, hydrogen-like s -state in the field of the positively charged donor. Since the motion of this electron is described in terms of the *effective* electron mass, which is small in semiconductors, its localization radius can be as large as 30 Å. Hence, its state may be controlled by relatively moderate electric fields. On the other hand, the exchange interaction between loosely bound electrons located on different donors results in a weak indirect coupling between their nuclear spins³, which coupling allows the implementation of, e.g., the quantum Control-Not operation.

A schematic illustration of the quantum computer proposed by Kane is shown in Fig. 1 for the particular case of two-qubits. Two ³¹P donors are implanted in silicon and subjected to an external dc magnetic field of about $B = 2T$. This creates a Zeeman splitting of the nuclear spin levels of about 3.5×10^7 Hz and a Zeeman splitting of electron levels of about 5.6×10^{10} Hz (much smaller than the splitting between the ground and the lowest excited hydrogen-like states of electron, which is^{4,5} 15 meV). The hyperfine coupling constant for Si:³¹P is 29 MHz. Since this constant is proportional to the probability of finding the electron near the nucleus, it can be decreased by effects that attract the electron away from

the ³¹P nucleus, which in the device depicted in Fig. 1 can be accomplished by applying a positive voltage to the “gates” labeled A_1 and A_2 . Similarly, the exchange interaction between the electrons located on different donors may be tuned by applying positive or negative voltage to the J -gate in Fig. 1, thereby changing the overlap of electron wave functions.

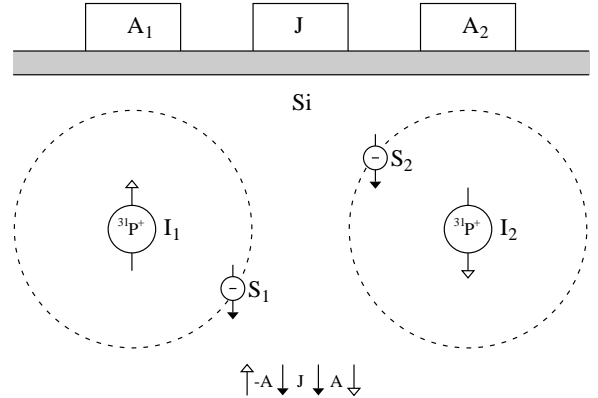


FIG. 1. Two ³¹P donors in silicon. The nuclear spins are coupled to the outer electrons by the hyperfine interactions, which can be controlled by the A gates. The electrons are mutually coupled via an exchange interaction, which can be controlled by the J gate.

In this article, we do not consider the actual *process* of quantum computation but instead focus on the *retrieval* of the result after the computation has been completed. The weak coupling of the nuclear spins with their environment, which is essential to avoid the decoherence that will spoil the quantum computation, makes this retrieval a highly nontrivial task. In particular, it cannot be accomplished by means of current NMR methods, since their sensitivity is as yet insufficient for detecting the signal from a single nuclear spin. Recognizing this, Kane proposed a special measurement procedure based on transferring the information about the *spin* state of the system to its *charge* state, where the result can be measured. In the following sections, we simulate numeri-

cally the measurement procedure proposed by Kane and estimate its optimal duration and minimum probability of error.

II. EIGENENERGIES AND EIGENSTATES

The Hamiltonian of the full system is

$$H = 2\mu_B B(\hat{S}_{1z} + \hat{S}_{2z}) - 2g_n\mu_n B(\hat{I}_{1z} + \hat{I}_{2z}) + 4A_1\hat{S}_1\hat{I}_1 + 4A_2\hat{S}_2\hat{I}_2 + 4J\hat{S}_1\hat{S}_2, \quad (1)$$

where \hat{S}_i and \hat{I}_i are electron and nuclear spin operators corresponding to donors $i=(1,2)$, μ_B (μ_n) is the Bohr (nuclear) magneton, $g_n = 1.13$ is the nuclear g -factor, B is the external magnetic field, A_i is the hyperfine interaction constant for nucleus i , and J determines the strength of the exchange interaction between the electrons.

The Hamiltonian H can be represented as a 16×16 matrix in the basis of states with definite electron and nuclear spin projections. Since the total spin projection in the field direction is conserved, all possible states fall into five invariant subspaces, corresponding to its values $-2, -1, 0, 1, \text{ and } 2$. In what follows, we will be interested only in the states with $S_{z\Sigma} + I_{z\Sigma} = -1$, which are used for measuring of the nuclear spin states. Hence we may focus on a reduced basis of four states: $|\downarrow\downarrow\rangle_e |\downarrow\uparrow\rangle_n$, $|\downarrow\downarrow\rangle_e |\uparrow\downarrow\rangle_n$, $|\downarrow\uparrow\rangle_e |\downarrow\downarrow\rangle_n$, and $|\uparrow\downarrow\rangle_e |\downarrow\downarrow\rangle_n$. In this reduced basis, the Hamiltonian can be represented by the 4×4 matrix

$$H = \begin{pmatrix} J - 2\mu_B B & 0 & 2A_1 & 0 \\ 0 & J - 2\mu_B B & 0 & 2A_2 \\ 2A_1 & 0 & 2g_n\mu_n B - J & 2J \\ 0 & 2A_2 & 2J & 2g_n\mu_n B - J \end{pmatrix}. \quad (2)$$

For simplicity, we henceforth assume that $A_1 = A_2 = A$. Then the Hamiltonian is symmetric with respect to donors 1 and 2, and the eigenstates are either symmetric or antisymmetric with respect to interchanging them. The two symmetric states, $|E_1\rangle$ and $|E_2\rangle$, have total electron and nuclear spins $\mathbf{S}_\Sigma = 1$ and $\mathbf{I}_\Sigma = 1$. The corresponding eigenenergies are given by

$$E_1 = g_n\mu_n B + J - \mu_B B + \sqrt{(\mu_B B + g_n\mu_n B)^2 + 4A^2}, \quad (3)$$

$$E_2 = g_n\mu_n B + J - \mu_B B - \sqrt{(\mu_B B + g_n\mu_n B)^2 + 4A^2}, \quad (4)$$

and the corresponding (unnormalized) eigenvectors are

$$|E_1\rangle = -(2g_n\mu_n B + J - E_1) |\downarrow\downarrow\rangle_e |\downarrow\uparrow + \uparrow\downarrow\rangle_n + 2A |\downarrow\uparrow + \uparrow\downarrow\rangle_e |\downarrow\downarrow\rangle_n, \quad (5)$$

$$|E_2\rangle = -(2g_n\mu_n B + J - E_2) |\downarrow\downarrow\rangle_e |\downarrow\uparrow + \uparrow\downarrow\rangle_n + 2A |\downarrow\uparrow + \uparrow\downarrow\rangle_e |\downarrow\downarrow\rangle_n, \quad (6)$$

The eigenenergies E_1 and E_2 are linear functions of J (see Fig. 2), and the structure of the corresponding eigenstates is independent of J (see Fig. 3).

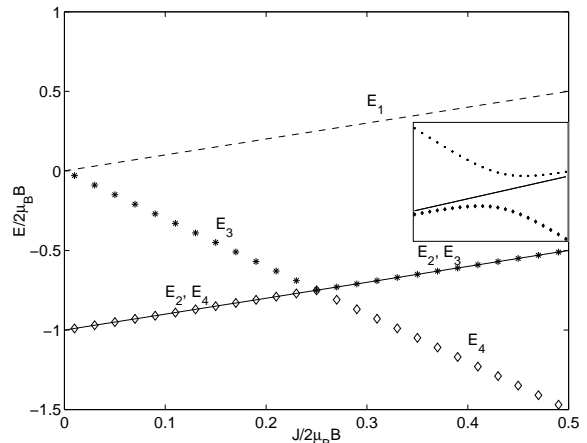


FIG. 2. Energy levels of the system of two coupled nuclear and electron spins versus exchange coupling J . The inset provides an expanded scale view of the avoided crossing (“bottleneck”) formed by $E_3(J)$ and $E_4(J)$ curves at $J = \mu_B B/2$.

The Hamiltonian H also has two antisymmetric states, $|E_3\rangle$ and $|E_4\rangle$, with total spin $\mathbf{S}_\Sigma + \mathbf{I}_\Sigma = 1$. The eigenenergies E_3 and E_4 are given by

$$E_3 = g_n\mu_n B - J - \mu_B B + \sqrt{(\mu_B B + g_n\mu_n B - 2J)^2 + 4A^2}, \quad (7)$$

$$E_4 = g_n\mu_n B - J - \mu_B B - \sqrt{(\mu_B B + g_n\mu_n B - 2J)^2 + 4A^2}, \quad (8)$$

and the corresponding (unnormalized) eigenvectors are

$$|E_3\rangle = -2A |\downarrow\downarrow\rangle_e |\downarrow\uparrow - \uparrow\downarrow\rangle_n - (2\mu_B B - J + E_3) |\downarrow\uparrow - \uparrow\downarrow\rangle_e |\downarrow\downarrow\rangle_n, \quad (9)$$

$$|E_4\rangle = -2A |\downarrow\downarrow\rangle_e |\downarrow\uparrow - \uparrow\downarrow\rangle_n - (2\mu_B B - J + E_4) |\downarrow\uparrow - \uparrow\downarrow\rangle_e |\downarrow\downarrow\rangle_n, \quad (10)$$

Unlike the energies of symmetric states, E_3 and E_4 are non-monotonic functions of J (see Fig. 2). If A were zero, the $E_3(J)$ and $E_4(J)$ curves would intersect at $J = \mu_B B/2$. However, since these terms have the same symmetry, they repel to form an avoided crossing (“bottleneck”) of width $4A$ at the would-be intersection point (see Fig. 2, inset). The corresponding eigenvectors also interchange character at this point. That is, as J increases from $J < \mu_B B/2$ to $J > \mu_B B/2$, $|E_3\rangle$ transforms from $|\downarrow\uparrow - \uparrow\downarrow\rangle_e |\downarrow\downarrow\rangle_n$ with $\mathbf{S}_\Sigma = 0$ and $\mathbf{I}_\Sigma = 1$ into $|\downarrow\downarrow\rangle_e |\downarrow\uparrow - \uparrow\downarrow\rangle_n$ with $\mathbf{S}_\Sigma = 1$ and $\mathbf{I}_\Sigma = 0$. In other words, the electron and neutron subsystems exchange their spins. Simultaneously, $|E_4\rangle$ undergoes the inverse transformation from $|\downarrow\downarrow\rangle_e |\downarrow\uparrow - \uparrow\downarrow\rangle_n$ into $|\downarrow\uparrow - \uparrow\downarrow\rangle_e |\downarrow\downarrow\rangle_n$, with the opposite spin transfer.

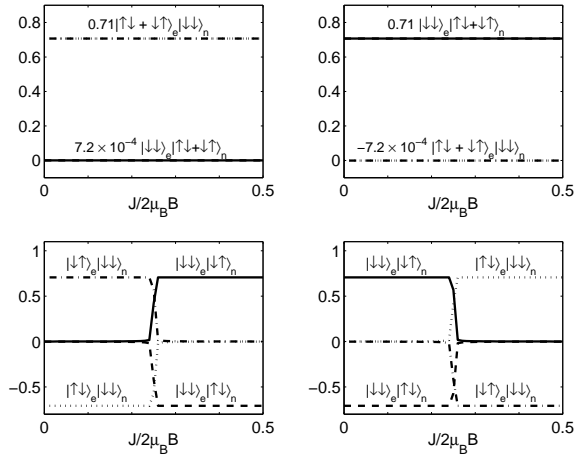


FIG. 3. The components of $|E_1\rangle$, $|E_2\rangle$, $|E_3\rangle$, and $|E_4\rangle$ states versus J .

One can thus distinguish between the singlet and triplet states of the nuclear subsystem as follows. Suppose that after the quantum computation has been performed with $J = 0$, the electron subsystem is in the $|\downarrow\downarrow\rangle_e$ state. Hence the whole system is either in $|E_2\rangle$ or in $|E_4\rangle$ state, depending on whether the nuclear subsystem is in the $|\downarrow\uparrow + \uparrow\downarrow\rangle_n$ or $|\downarrow\uparrow - \uparrow\downarrow\rangle_n$ state. If the exchange parameter is then adiabatically increased to $J \gg \mu_B B/2$, the final electron subsystem is (respectively) a triplet or singlet state, thus allowing the information to be transferred from the nuclear to the electron spin subsystem. To complete the measurement, one can distinguish between these electron spin states through the difference in their charge properties, as described by Kane¹.

III. SIMULATIONS OF THE MEASUREMENT DYNAMICS

To simulate the dynamics of measurement, we solve numerically the equation

$$\frac{d\rho}{dt} = \frac{i}{\hbar}[\rho, \mathcal{H}(t) + \delta\mathcal{H}(t)], \quad (11)$$

where ρ is the 4×4 density matrix of the system, $\mathcal{H}(t)$ is given by (1) with $J(t)$ linearly increasing from 0 to $2\mu_B B$. We allow for a fluctuating correction

$$\delta\mathcal{H} = 4\delta A_1(t)\hat{\mathbf{S}}_1\hat{\mathbf{I}}_1 + 4\delta A_2(t)\hat{\mathbf{S}}_2\hat{\mathbf{I}}_2 \quad (12)$$

to account for the voltage noise of the A-gates. The random classical quantities δA_1 and δA_2 are assumed to have correlation time τ_c much shorter than all the dynamic time scales and zero averages. Following Abragam⁶, we rewrite the equation for the density matrix in the form

$$\frac{d\rho}{dt} = -\frac{i}{\hbar}[\mathcal{H}, \rho] - \frac{\tau_c}{\hbar^2} \overline{[\delta\mathcal{H}(t), [\delta\mathcal{H}(t), \rho]]}, \quad (13)$$

where overlining denotes averaging over realizations of the fluctuations. We estimate the spectral density of

fluctuations of A_1 and A_2 using the spectral density of voltage fluctuations for room-temperature electronics $S_V = 10^{-18} \text{ V}^2/\text{Hz}$ and $d(A/h)/dV \sim 30 \text{ MHz/V}$ (see Ref. 1). The system is initially prepared in the $|E_4\rangle$ state.

Figure 4 shows the time dependences of occupation probabilities of the eigenstates $|E_1\rangle - |E_4\rangle$ during the measurement process.

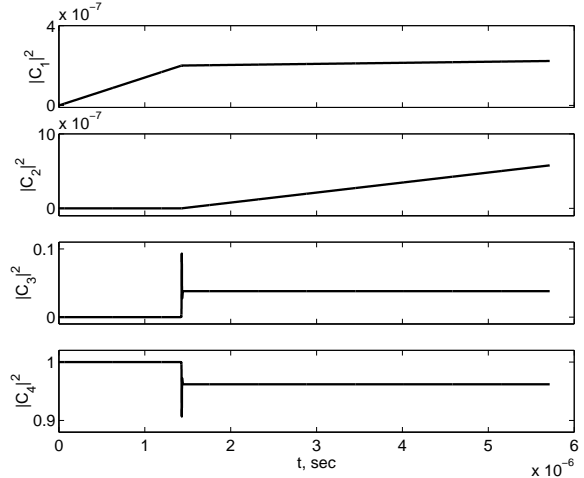


FIG. 4. The time evolution of the occupancies of $|E_1\rangle - |E_4\rangle$ states during the measurement. The duration of measurement is $T = 5.7 \times 10^{-6}$ sec, the hyperfine interaction constant is $A/h = 2.9 \times 10^7$ Hz, and the noise spectral density is $S_A/h^2 = 3.5 \times 10^{-3}$ Hz.

In this figure, we have taken the duration of measurement to be $T = 5.7 \times 10^{-6}$ sec, the hyperfine interaction constant to be $A/h = 2.9 \times 10^7$ Hz, and the noise spectral density to be $S_A/h^2 = 3.5 \times 10^{-3}$ Hz. It is readily seen that increasing J at a finite rate results in a finite probability of exciting the system from $|E_4\rangle$ into $|E_3\rangle$, creating one source of measurement error. Another source of error is noise-induced “escape” into the eigenstates $|E_1\rangle$ and $|E_2\rangle$. Note that the system cannot be excited into these states in the absence of noise because of their different symmetry. Since the fluctuations of A_1 and A_2 violate the symmetry with respect to donors 1 and 2, they make this excitation possible. The different shapes of curves representing $|C_1(t)|^2$ and $|C_2(t)|^2$ are explained by the “restructuring” of the eigenstate $|E_4\rangle$ state at $J = \mu_B B/2$: the noise-induced transitions are accompanied by flipping one nuclear and one electron spin in opposite directions. The noise also contributes to the escape to $|E_3\rangle$.

Figure 5 depicts the dependence of final amplitude of $|E_4\rangle$ on the duration of measurement (solid curve).

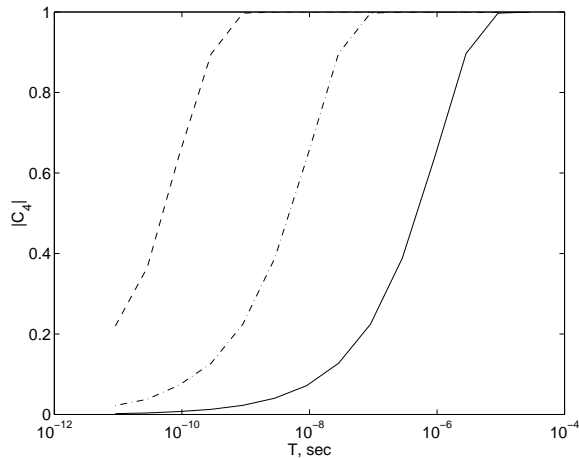


FIG. 5. The amplitude of $|E_4\rangle$ versus the duration of measurement for $B = 2$ Tesla and $A/h = 2.9 \times 10^7$ Hz (solid curve). The dash-dotted and dashed curves show the same dependences for $A/h = 2.9 \times 10^8$ Hz and $A/h = 2.9 \times 10^9$ Hz, respectively.

For small T , $|C_4|^2 \rightarrow 0$ because the short-time dynamics of the electrons is only weakly affected by the hyperfine interaction, and the electron subsystem retains its spin during the course of the measurement. For sufficiently large T , P_4 tends to 1 according to the law $1 - |C_4|^2 \propto \exp(-T/\tau)$. For representative values of $B = 2$ Tesla and $A/h = 2.9 \times 10^7$ Hz, one obtains $\tau^{-1} = 5.7 \times 10^5 \text{ sec}^{-1}$.

To understand why τ^{-1} is three orders of magnitude smaller than A , we calculated the same curve for $A/h = 2.9 \times 10^8$ Hz and $A/h = 2.9 \times 10^9$ Hz (dash-dotted and dashed curves). Figure 6 shows the logarithmic plot of τ^{-1} vs A .

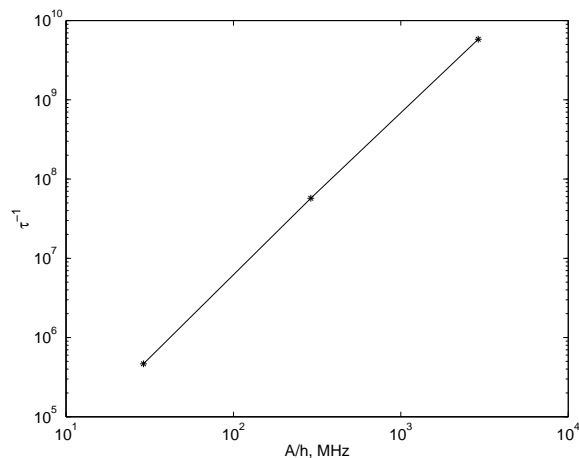


FIG. 6. The characteristic time τ versus the hyperfine interaction constant A .

By scaling A , we found that $\tau^{-1} \propto A^2/2\mu_B B\hbar$. This result can be readily explained. The width of the gap between the states $|E_4\rangle$ and $|E_3\rangle$ is $\Delta E = 4A$ (see Fig. 2, inset), and the corresponding interval of J is also of the order of A . Hence the result that $\tau^{-1} \propto A^2$ follows

from noting that $T/\tau \sim \Delta E/\hbar \Delta t$, where $\Delta E \propto A$ and Δt , which is the time of passage of the system through the “bottleneck” region, is also proportional to A , since J is ramped up linearly in our simulation.

If it were not the gate-voltage noise, the measurement error could be made vanishingly small just by increasing the duration of measurement. However, because of noise, the error passes through a minimum as a function of duration and then increases again. The details of behavior of the measurement error are shown in Fig. 7.

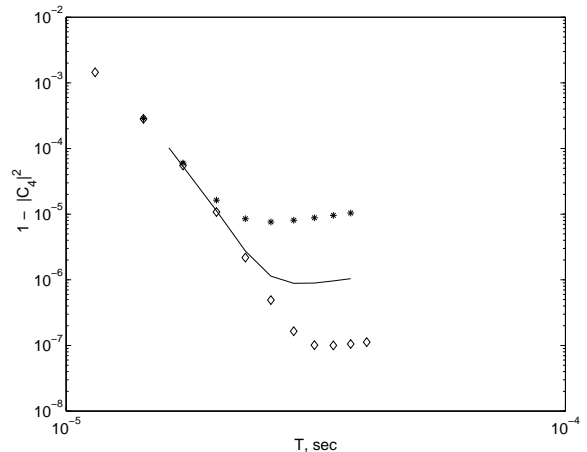


FIG. 7. The measurement error, $1 - |C_4|^2$, versus the duration of measurement for different levels of gate-voltage noise: $S_A/h^2 = 3.5 \times 10^{-3}$ Hz (*), 3.5×10^{-4} Hz (solid line), and 3.5×10^{-5} Hz (\diamond).

The minimum error $(1 - |C_4|^2)_{min}$ is proportional to the noise spectral density S_A (see Fig. 8) and is of the order of 10^{-6} for typical values of noise.

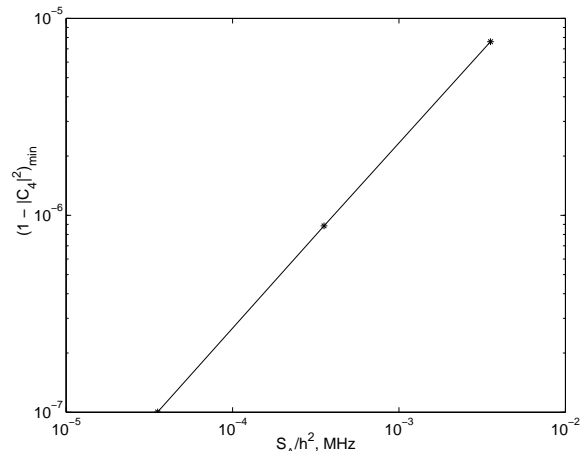


FIG. 8. The minimum attainable measurement error versus the noise spectral density.

IV. ACKNOWLEDGEMENTS

It is a pleasure to thank Chris Hammel, Bruce Kane, and Denis Pelekhov for valuable discussions. K.E.N. is

grateful to the Theoretical Division and the CNLS of the Los Alamos National Laboratory for their hospitality. This work was supported by the Department of Energy under contract W-7405-ENG-36, by the National Security Agency, and by Linkage Grant 93-1602 from the NATO Special Programme Panel on Nanotechnology.

¹ B.E. Kane, *Nature* **393**, 133 (1998).

² J.S. Waugh and C.P. Slichter, *Phys. Rev. B* **37**, 4337 (1988).

³ C.P. Slichter, *Principles of Magnetic Resonance*, Springer, 1996.

⁴ R. Enderlein, N.J.M. Horing, *Fundamentals of Semiconductor Physics and Devices*, World Scientific, 1997.

⁵ W. Kohn, *Solid State Physics*, Vol. 5, (Eds: F. Seitz, D. Turnbull), Academic, New York, 1957.

⁶ A. Abragam, *The Principles of Nuclear Magnetism*, Oxford University Press, 1961.